GEN Biotechnology
Volume 1, Number 1, 2022

DOI: 10.1089/genbio.2021.0011

GEN Biotechnology

RESEARCH ARTICLE

Competitive Displacement of *De Novo* Designed HeteroDimers Can Reversibly Control Protein–Protein Interactions and Implement Feedback in Synthetic Circuits

Taylor H. Nguyen,[1,†] Galen Dods,[1,†] Mariana Gómez-Schiavon,[1–3] Muziyue Wu,[1,4,5] Zibo Chen,[6–8] Ryan Kibler,[6–8] David Baker,[6,7,9] Hana El-Samad,[1,10,11,*] and Andrew H. Ng[1,10,12,*]

Abstract

Dynamic dimerization is a common regulatory interaction between biological molecules, underpinning many signaling functions. Because of its ubiquity, many biological engineering efforts have focused on building dimerizing proteins, such as the SYNZIPs and *de novo* Designed HeteroDimers (DHDs). Using the DHDs as a model system, we show that low-affinity protein interactions can be competitively displaced by a high-affinity "dominant negative" heterodimer. We demonstrate the utility of this signaling motif by using competitive displacement to implement negative feedback in a synthetic circuit. Competitive displacement could be extended to other heterodimer systems to expand the functionality of protein circuits and enable new biotechnology applications.

Introduction

Biotechnology often draws inspiration from the natural world to inform the design of strategies for regulating biology. Proteins play a central role in transmitting information in biological systems, and thus their regulation is a major thrust of synthetic biology. Protein–protein interactions play a critical role in regulating signal transduction.[1] Many transcription factors (TFs) utilize dimerization to control their activity, such as basic helix-loop-helix (bHLH) proteins, which play important roles in differentiation and whose dysregulation can cause cancer.[2] One such bHLH, MyoD, can either homodimerize or heterodimerize with other bHLHs, including E47 and E12, to activate transcription. Other bHLHs, including Group D bHLHs, contain the HLH domain needed for dimerization but lack the basic region needed for transcriptional activation. Consequently, Group D proteins can bind other bHLHs to negatively regulate their activity.

For example, the Group D Id protein is able to preferentially bind MyoD, E47, or E12 to attenuate their ability to bind DNA, thus repressing their transcriptional programs.[3,4] The relative abundances of these proteins determine the differentiation state of muscle cells. This example showcases how both transcriptional activation and repression can be highly regulated through the joining and competition of TF dimerization. Such protein–protein interactions are, therefore, promising engineering targets for achieving complex and novel cellular functions.

Although protein-based circuits are ubiquitously used for endogenous biological regulation, methods for synthetic modulation of protein–protein interactions remain limited. Previous work in synthetic biology has focused on using high-affinity binders to create activation signals. This highly modular strategy can be used to reconstitute split proteins or colocalize signaling molecules. This functionality has enabled the control of

Departments of [1]Biochemistry and Biophysics and [12]Cellular and Molecular Pharmacology, University of California, San Francisco, San Francisco, California, USA; [2]Laboratorio Internacional de Investigación sobre el Genoma Humano, Universidad Nacional Autónoma de México, Santiago de Querétaro, México; [3]ANID—Millennium Science Initiative Program—Millennium Institute for Integrative Biology (iBio), Santiago, Chile; [4]Graduate Program of Biophysics, University of California, San Francisco, San Francisco, California, USA; [5]Cardiovascular Research Institute, University of California, San Francisco, San Francisco, California, USA; [6]Department of Biochemistry, University of Washington, Seattle, Washington, USA; [7]Institute for Protein Design, University of Washington, Seattle, Washington, USA; [8]Graduate Program in Biological Physics, Structure, and Design, University of Washington, Seattle, Washington, USA; [9]Howard Hughes Medical Institute, University of Washington, Seattle, Washington, USA; [10]Cell Design Initiative, University of California, San Francisco, California, USA; [11]Chan–Zuckerberg Biohub, San Francisco, California, USA; and [12]Department of Cellular and Molecular Pharmacology, University of California, San Francisco, San Francisco, California, USA.
[†]Cofirst authors.

*Address correspondence to: *Hana El-Samad, Department of Biochemistry and Biophysics, University of California, San Francisco, 1700 4th St., San Francisco, CA 94158, USA,* E-mail: hana.el-samad@ucsf.edu; *Andrew H. Ng, Department of Biochemistry and Biophysics, University of California, San Francisco, 1700 4th St., San Francisco, CA 94158, USA,* E-mail: a.ng305@gmail.com

transcription, localization, and proteolysis[5–10]; the tuning of ultrasensitivity and cooperativity[11–15]; the rewiring of endogenous signaling pathways[16–19]; the optimization of metabolic pathways[20–22]; and the modulation of CAR activity and downstream T cell responses.[23,24]

Many of these applications utilize SYNZIPs, which are a library of highly characterized synthetic bZIP proteins.[25] However, far less work has been dedicated to building inhibitory binding reactions that can interrupt the function of the dimerized partners, like those seen in endogenous pathways. Furthermore, inhibitory binding could be used in synthetic circuits to tune dose responses or implement composable negative regulation and feedback, enabling the construction of complex circuits that more closely approximate endogenous signaling.

Recently, a library of *de novo* Designed HeteroDimers (DHDs) was computationally designed using Rosetta HBNet.[26] Each heterodimer pair shares the same four-helix bundle backbone structure, and specificity was achieved by incorporating asymmetric hydrogen bond networks into the backbone. Monomers were generated by using short loops to connect pairs of helices, and six heterodimer pairs were observed to be fully orthogonal through a yeast two-hybrid assay. Each designed pair is referred to by a number, and each monomer within a pair is designated as A or B, that is, 37A and 37B make up the designed 37 on-target interaction. The functionality of the DHD library was demonstrated through the construction of multicomponent protein logic gates that regulate split-protein activity and transcription in yeast and T cells.[24]

In this study, we extend the functionality of the DHD library by demonstrating that the binding of the dimerized partners can be reversed. Specifically, we show that dominant negative (DN) heterodimers can competitively displace weaker interactions to implement negative regulation of split proteins. We first present an extended characterization of a subset of the DHD library using a titratable[27,28] split TF system. Using a selection of four DHD pairs, we study all possible combinations of interactions between individual DHD monomers and identify several novel low-affinity off-target interactions.

We show that these low-affinity interactions can be competitively displaced by introducing the on-target high-affinity heterodimer, referred to here as the "dominant negative" (DN). We characterize the properties of the DN and dynamics of competitive displacement, and use this information to design a negative feedback circuit that utilizes a DN to implement negative regulation. The application of competitive displacement to control other split proteins offers a promising strategy that could greatly expand the scope of protein circuits for a variety of biotechnology and therapeutic applications.

Results

Quantification of DHD interaction affinities

Previous characterization of the DHDs was carried out using a yeast two-hybrid system. Canonical yeast two-hybrid systems detect protein–protein interactions through dimerization-dependent activation of an auxotrophic marker. Although this assay is useful for rapidly screening protein interaction pairs, colony formation or cell growth is typically binary and does not necessarily inform relative binding affinity. The rational design of protein-based circuits requires a quantitative understanding of relative protein affinities in a cellular context.

To achieve this quantification, we developed a fluorescence-based split TF assay in *saccharomyces cerevisiae*. We fused DHDs to either a synthetic zinc-finger ZF43_8 DNA-binding domain (DHD-DBD or DHD-ZF43_8) or VP16 activation domain (DHD-AD or DHD-VP16).[14] Interaction between the DHDs reconstitutes the ZF43_8-VP16 TF and activates the cognate p43_8 promoter to drive expression of a yellow fluorescent protein (YFP) reporter (Fig. 1A).

We utilized two orthogonal drug-inducible systems (GEM, a fusion of Gal4 DBD, estradiol ligand binding domain, Msn2 AD, and Z3PM, a fusion of Z3 DBD, progesterone ligand binding domain, Msn2 AD)[27,28] to express different levels of the DHD–DBD fusion and the DHD–AD fusion. The GEM synthetic TF is induced by estradiol (E2) to activate the pGAL1 promoter and produce the DHD–DBD fusion. The Z3PM synthetic TF is activated by the orthogonal drug progesterone (Pg) to induce the pZ3 promoter and produce the DHD–AD fusion.

We first investigated the optimal orientation for fusing a DHD to either ZF43_8 or VP16. We fused the 37B monomer to VP16 and the cognate 37A monomer to ZF43_8 and measured the YFP expression of all four combinations of N- and C-terminal fusions. We saturated expression of the DBD species and measured YFP expression in the presence and absence of the AD species. We observed the largest dynamic range when fusing both DHDs to the N-termini of VP16 and ZF43_8 (Fig. 1B). Given the common structure of the DHDs, we assumed that the N-terminal fusions would be optimal for all other DHDs and thus used this configuration for all other experiments.

To test the full dynamic range of our assay, we performed a two-dimensional induction wherein we independently titrated the expression of the DHD–ZF43_8 and DHD–VP16 fusions for both the 37 and 154 DHD on-target pairs (Fig. 1C). In the absence of both inducers, we observed minimal YFP expression. As expected, YFP expression increased with increasing amounts of Pg (DHD–VP16). Interestingly, for low to intermediate concentrations of Pg (DHD–VP16), YFP expression decreased with increasing amounts of E2 (DHD–ZF43_8). YFP expression was insensitive to increasing E2 at high concentrations of Pg. We hypothesized that this paradoxical effect may be a result of excess free DHD–ZF43_8 acting as a transcriptional repressor by competing for promoter occupancy with the bound DHD–ZF43_8:DHD–VP16 complex.

To explore this hypothesis, we proposed a simple *promoter occupancy competition model* based on the system shown in Figure 1A. This model considers that the regulated promoter can exist in three states: unbound/free (with basal transcriptional activity inherent to the promoter), bound to the DHD TF (with full transcriptional activity), or bound to the free DBD species (without transcriptional activity; see Supplementary Data for full description). In the *competition model*, the amount of free DBD species effectively represses the transcriptional activity by competing for the promoter binding site (Supplementary Fig. S1A).

For comparison, we also built a *no-competition model* in which the effect of the free DBD species on promoter transcriptional activity is assumed to be negligible and is excluded from the model (i.e., only two promoter states, unbound/free and bound to the DHD TF, are considered; Supplementary Fig. S1B). For a wide range of parameter values, the *competition model* displays the paradoxical effect observed in Figure 1C: increasing the DBD part expression by increasing E2 concentration reduces the YFP reporter expression for low or medium Pg concentrations (Supplementary Fig. S1A).

This behavior was never observed in the *no-competition model*; increasing E2 resulted in higher YFP expression for all explored parameter values (Supplementary Fig. S1B). This result suggests that the most parsimonious model of promoter competition is sufficient to explain the data, and highlights the need to characterize synthetic parts over large dynamic ranges to be able to use them predictably for circuit construction.

With this information at hand, we next sought to determine the relative strengths of interactions between different DHD parts, testing a matrix of on-target and off-target pairs. We chose a subset of four on-target DHD pairs (37A/B, 13A/B, 154A/B, and 155A/B) and constructed strains for all possible 64 combinations of on- and off-target pairings in our split TF assay. We then measured YFP expression in the presence of saturating concentrations of both hormone inducers (Supplementary Fig. S2B) and absence of both inducers (Supplementary Fig. S2A). We used these two values to calculate the fold-change YFP expression upon induction of both DHD–VP16 and DHD–ZF43_8 (Fig. 1D).

We noticed activation of the split TF was not symmetric for all DHD pairs. For both the 37 and 155 DHD on-target interactions, the split TF was only active when the DHD A monomer was fused to ZF43_8 and the B monomer was fused to VP16. We speculate that the asymmetry could be a function of structure–function changes with fused proteins,[29,30] and these observations helped inform our downstream circuit design.

In addition to the on-target interactions, we observed several interactions of varying strengths among off-target DHD (DHDoff) pairs, of which only the 13B/37B interaction was previously identified through growth-based two-hybrid characterization.[26] Our assay also revealed a range of binding activities for some DHDs to multiple DHDoffs. For example, 154B-ZF43_8 interacted with 37A-VP16 weakly, with 13B-VP16 moderately,

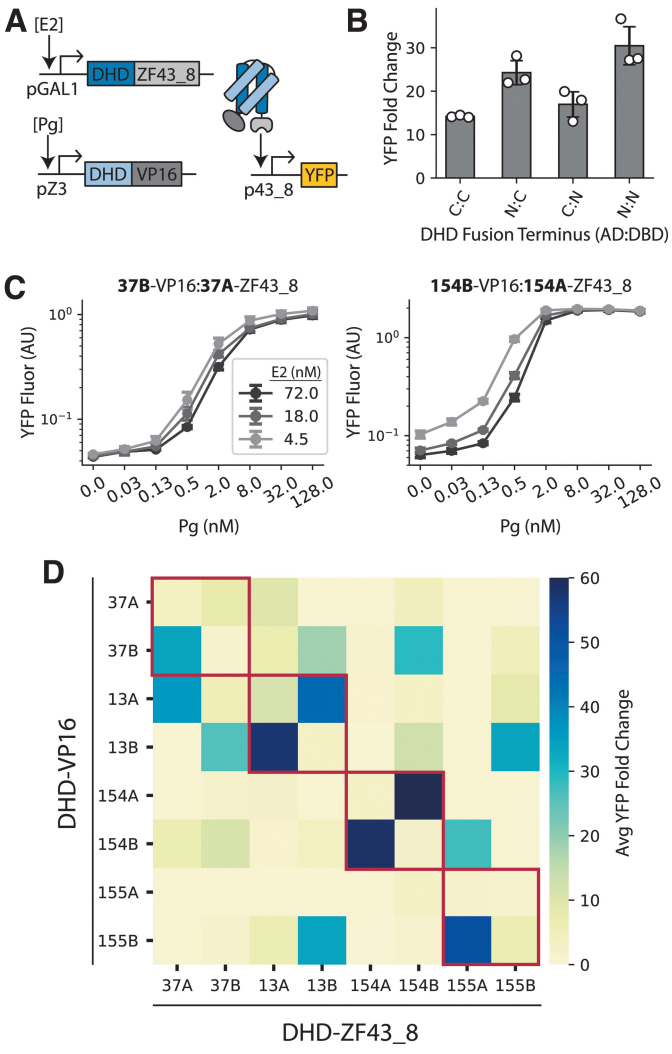

FIG. 1. A split TF system enables the quantification of DHD interactions through fluorescence.

(A) Cartoon of the split TF system. Different DHDs are fused to the ZF43_8 and VP16 species, and these are induced by the addition of E2 and Pg, respectively. Interacting DHDs reconstitute the TF complex and induce YFP (Venus) expression from the cognate promoter (p43_8).

(B) YFP fluorescence generated by the reconstitution of the split TF using different termini fusions of the 37B:37A pair. The label of "N:N" denotes the orientation where both DHDs were fused to the N-termini of VP16 (AD) and ZF43_8 (DHD), whereas "N:C" denotes the orientation where DHD is fused to the N-terminus of VP16 (AD) and the C-terminus of ZF43_8 (DBD). Constructs were induced with a saturating dose of 36 nM E2 and 256 nM Pg. Steady-state YFP measurements at 6 h post-induction are reported. Values represent the mean and SD of three biological replicates.

(C) YFP fluorescence dose response as a function of Pg for the 37 (left) and 154 (right) DHD pairs at select values of E2. Both cases show a decrease in expression with increasing amounts of the DBD species (E2 amount). Values represent the mean and SD of three biological replicates and data were collected 6 h after E2 and Pg induction.

(D) All-by-all interaction matrix for four DHD pairs. Designed interactions are outlined in red. Values represent the mean YFP fold-change between when both species are induced (72 nM E2 and 128 nM Pg) and neither species is induced (0 nM E2 and Pg). Data were collected 6 h after E2 and Pg induction. Values represent the mean of three biological replicates. AD, activation domain; DHD, Designed HeteroDimers; E2, estradiol; Pg, progesterone; SD, standard deviation; TF, transcription factor; YFP, yellow fluorescent protein.

and with 37B-VP16 strongly. Nonetheless, the designed interaction partner always displayed the strongest split TF activation for a given DHD.

Characterization of DN interactions

Given the full interaction matrix, we hypothesized that a high-affinity on-target interaction, which we refer to as the DN, might be able to inhibit and potentially reverse interactions between weaker DHD pairs, enabling new functionality in heterodimer-based circuits. To test this hypothesis, we selected 154A as a model DN because it exhibited a range of interaction strengths with other DHDs (Fig. 1D). We then built a new circuit in which E2-induced pGAL1 drives expression of both 154B-VP16 and a DHDoff: 155A-ZF43_8, 37B-ZF43_8, or 37A-ZF43_8, ordered in decreasing binding affinity for 154B in this orientation (Fig. 2A).

The reconstituted split TF activates the p43_8 promoter to drive expression of an YFP-cODC degron fusion; the degron enables more rapid turnover of the circuit to more efficiently capture the displacement phenomenon.[31] Concurrently, Pg-induced pZ3 drives expression of 154A, which acts as the high-affinity DN for 154B to potentially inhibit the split TF interaction. In a different permutation of the circuit designed to check for fusion effects, 154B was fused to ZF43_8 instead of VP16, and pGAL1 drives expression of both 154B-ZF43_8 and a DHDoff: 37B-VP16, 13B-VP16, and 37A-VP16, ordered in decreasing binding affinity for 154B in this orientation (Fig. 2B).

To test the ability of DN to compete with heterodimer formation, we simultaneously induced cells with a saturating dose of E2 and a range of Pg concentrations (Fig. 2C). We then measured YFP fluorescence 6 h later. We observed that expression of the DN indeed reduced YFP expression by inhibiting the weak-affinity active TF through the formation of high-affinity inactive complexes (Fig. 2D, E).

Interestingly, we found that a higher concentration of the 154A DN was required to fully inhibit the split TF when 154B was fused to VP16 (Fig. 2D) than when 154B was fused to ZF43_8 (Fig. 2E). When the DN bound 154B-ZF43_8, YFP expression dropped off precipitously with small amounts of Pg (Fig. 2E). This difference cannot be explained simply by the promoter competition of inactive DBD parts (either free or bound to the DN part) as in the *competition model* already proposed, because the total concentration of the promoter binding (hence repressive) species in both circuit configurations is the same and determined by the E2 concentration (Fig. 2A, B).

However, our model shows that varying either the binding rates between on-target species (i.e., between DN and the sequestered part, either AD or DBD) or the expression level of the parts can shift the dose response just as observed with the tested designs, suggesting that alternative fusion arrangements for 154B may alter its binding affinity to the DN or the expression level of the parts (Supplementary Fig. S3; Fig. 2D–E; see Supplementary Data for full description). Our experimental testing of DHD interactions shown in Figure 1D supports this hypothesis; we previously observed that the same pair of DHDs could display different affinities depending on whether the monomer was fused to AD or DBD.

Although this first assay tested the ability to form high-affinity complexes in the presence of weak-affinity binders, the application of the DN to dynamic signaling circuits requires the ability to displace existing complexes. Using the same circuits, we next investigated whether the 154A DN would be able to competitively displace the weaker DHDoff bound to 154B after the DHDoff and 154B pair reached binding equilibrium. To do so, we induced one circuit from each layout (Fig. 2A, B) with a saturating dose of E2 for 4 h to express both parts of the split TF, leaving ample time for the split TF to reach equilibrium and form active complexes.[27]

After 4 h of such E2 induction, we induced cells with a saturating dose of Pg to activate production of 154A DN and measured YFP fluorescence over another 4 h period (Fig. 2F). To enable comparison between the two circuit layouts, we normalized YFP fluorescence by subtracting the background fluorescence and dividing by the maximum fluorescence output of each circuit. We observed a decrease in YFP fluorescence for both circuits within 1 hour of DN induction (Fig. 2F). The rapid decay in transcriptional output suggests that the DN can inhibit the split TF even after the weak-affinity DHDs have reached binding equilibrium.

Moreover, the 154A DN deactivated the split TF faster for 154B-ZF43_8 than for 154B-VP16. This result is in agreement with our previous observation that 154A is a more potent DN when creating 154A:154B-ZF43_8 complexes. These experiments demonstrate that DN DHD interactions can be a powerful tool for reversible regulation of the activity of split proteins and outline several parameters for tuning the strength and dynamics of this inhibitory reaction.

Development of a negative feedback circuit using competitive displacement

To capitalize on the ability of the DHDs to dynamically assemble and interchange components, we sought to use it in a genetic circuit. Specifically, we reasoned that the interruption of the split TF through formation of a DN interaction could be used to build a modular negative feedback structure in a circuit simply by producing the DN part from the output of this circuit (Fig. 3A). To test this idea, we built a circuit in which the synthetic TF GEM (induced by E2) activates the pGAL1 promoter to produce both parts of a split TF (154B-VP16 and 155A-ZF43_8 species).

When the split TF heterodimer forms, it activates the p43_8 promoter to produce an intermediate reporter red fluorescent protein (RFP), as well as the synthetic TF Z3PM. Z3PM in turn activates the pZ3 promoter to drive expression of the DN 154A, implementing negative feedback by binding to 154B-VP16 and inhibiting the formation of the split TF. Z3PM also binds to another copy of the pZ3 promoter to transcribe two copies of an YFP-cODC output. Z3PM and RFP are fused to a photosensitive degron (psd), which acts as a weak degron. With the cODC degron, the DN will have a similar turnover rate as the YFP to more closely approximate the output of the circuit.

At a given concentration of E2 and Pg, the system settles at a given steady state. In the presence of feedback, increasing Pg

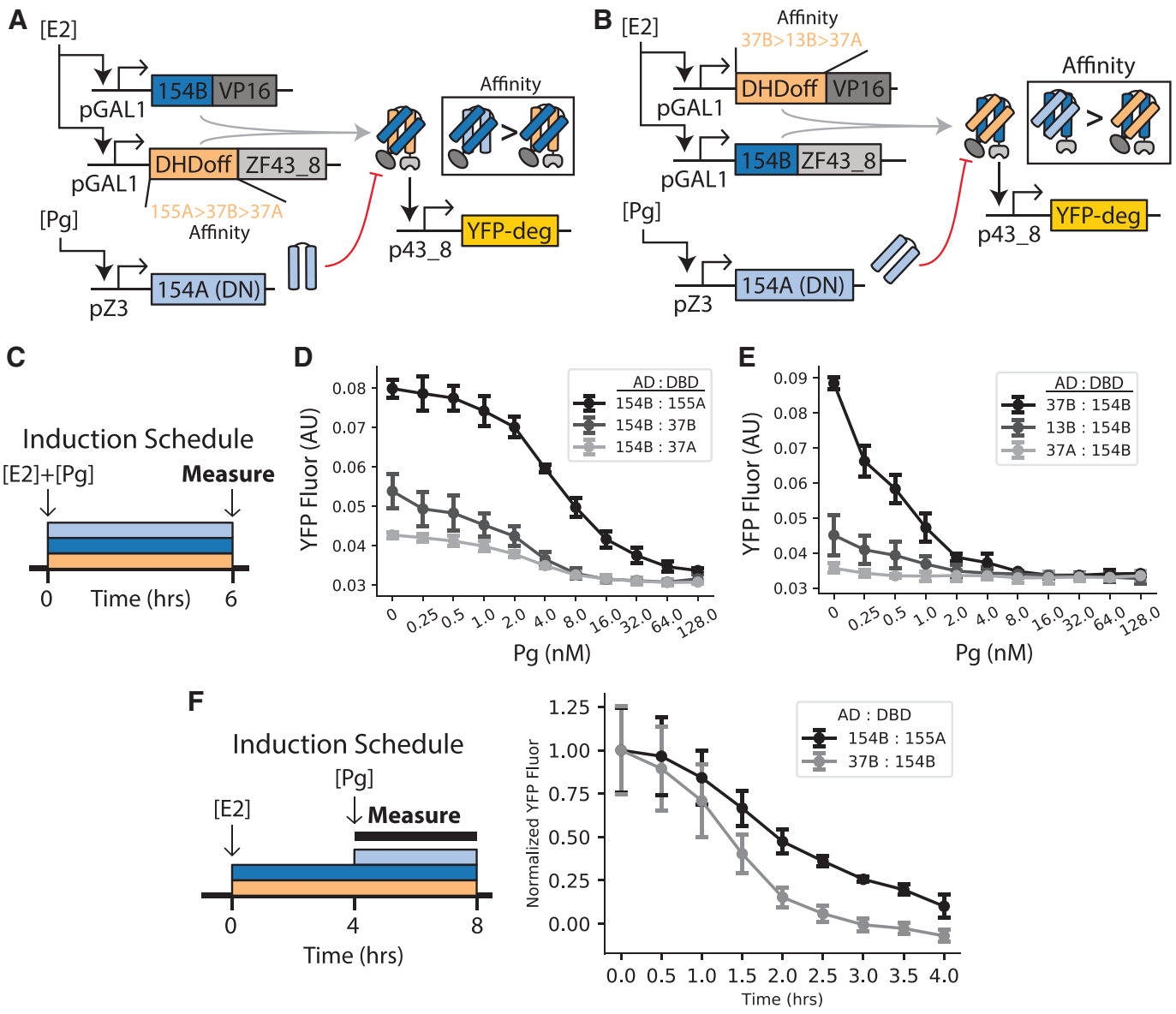

FIG. 2. Characterization of competitive displacement through DHD DNs.

(A, B) Cartoons of the system used to test the DN. E2 induces the production of the off-target interacting DHDs that reconstitute the TF. Pg induces the production of DN that can outcompete the bound DHDs. The DN interferes with complex formation or integrity by binding to either the AD **(A)** or DBD **(B)** species, and, therefore, turns off YFP-cODC degron expression observed through a decrease in YFP fluorescence. **(C)** Left, timeline of inductions. Both E2 and Pg are given at time 0 and YFP expression was measured 6 h after induction.

(D, E) Steady-state responses of each circuit layout in **A** and **B**, respectively. Each strain is given a saturating amount of E2 (36 nM) and a range of Pg concentrations.

(F) Left, timeline of inductions. E2 is given at time 0 allowing the DHD complex to form, whereas Pg is given 4 h later to test whether the DN can interfere with the complex. YFP expression was measured 8 h after induction with E2 (4 h after induction with Pg). Right, YFP fluorescence as a function of time for each layout in panels **A** and **B** (37B:154B in grey, DN is 154A and 154B:155A in black, DN is 154A). The data show DN can displace preformed complexes as evidenced by a decrease in YFP fluorescence. Measurements were taken every 30 min for 4 h beginning immediately after Pg induction. YFP expression was normalized by the expression at time 0. For all panels, values represent the mean and SD of three biological replicates. The lines connecting points were added to aid visualization. DN, dominant negative.

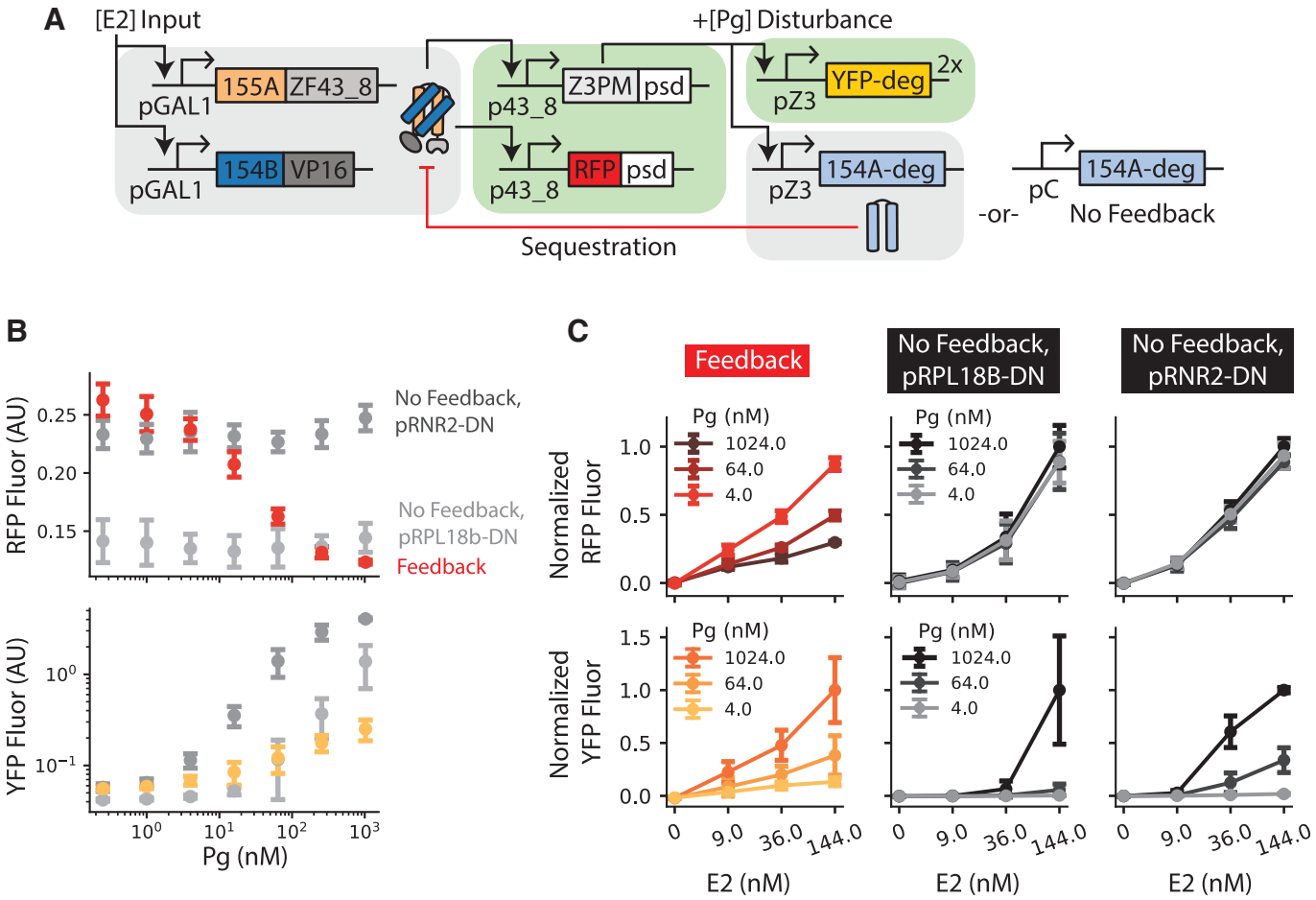

FIG. 3. Design and implementation of a negative feedback circuit using DN competitive displacement.

(A) Schematic of the synthetic feedback circuit implemented with the competitive displacement strategy. E2 acts as the input and induces expression of the DHD TF complex. The TF then induces the production of Z3PM and RFP (an internal readout of TF activity). Z3PM in turn induces expression of the 2× YFP output (YFP-cODC increases the turnover rate of YFP to degrade old YFP molecules and approximate current YFP output). The feedback circuit produces the DN (DN-cODC degron) from the pZ3 promoter. The feedback circuit is compared with two no feedback circuits where the DN-cODC is produced from a pC. pC can either be pRPL18B (noted as pRPL18B-DN) or a pRNR2 (noted as pRNR2-DN) in subsequent panels.

(B) RFP and YFP values after 8 h of circuit induction for an input E2 of 144 nM, plotted as a function of Pg. Shown are the feedback (red and yellow) and no feedback data (light gray for pRPL18B-DN and dark gray for pRNR2-DN).

(C) The output of the feedback circuit can be tuned with different E2 inputs. Feedback (red and yellow) and both no feedback (grays) circuits were induced with a full range of E2 and Pg for 8 h. Fluorescence values were normalized to the maximum fluorescence value of each channel of each circuit, to allow for comparisons between circuits with different dynamic ranges. Lines were added to aid visualization. All values represent the mean and SD of three biological replicates. PC, constitutive promoter; RFP; Z3 DBD, progesterone ligand binding domain, Msn2 AD.

disturbs the system from its steady state. This increase should also increase DN expression, which can compensate for the Pg disturbance by inhibiting the split TF and decreasing the production rate of Z3PM and RFP. For comparison, we also constructed two "no feedback" controls that express the DN using two constitutive promoters (pCs) with different strengths.

We first investigated whether the feedback circuit and its no-feedback control imposed a growth burden on yeast. To do so, we induced cells with a saturating concentration of E2 and Pg, and compared the growth of cells harboring the circuit with the growth of the background strain for 24 h (Supplementary Fig. S4). There was no observable difference in growth at any inducer combination. Interestingly, cells harboring the circuits grew faster than the background strain, likely due to the prototrophy conferred by integrating the circuit components.

To assess the properties of the feedback circuit, we compared the responses of the circuits with and without feedback as a function of Pg for a fixed concentration of E2 (144 nM E2; Fig. 3B and Supplementary Fig. S5). In both "no feedback" circuits, the YFP output increases unabatedly as Pg increases. In

addition, the RFP remains constant, as the DN production is, by design, fixed and insensitive to Pg. By contrast, the feedback circuit increased production of the DN with increasing Pg. As expected, increasing DN inactivated more split TF, reducing activity of the p43_8 promoter, which was apparent as a decreasing RFP fluorescence (a proxy for decreasing Z3PM).

The decreasing Z3PM concentration compensates for the higher Pg, thereby controlling the effect of this disturbance on the YFP output (Fig. 3B). In contrast, different constitutive levels of expression of the DN in the various "no feedback" circuits were unable to recapitulate buffering against high Pg disturbances, highlighting the unique properties of the feedback circuit (Fig. 3B and Supplementary Fig. S5). To test our general understanding of the strategy of the feedback circuit and its qualitative properties, we built a computational model that recapitulated the behavior of the experimental results using the same parameters used in the previous models (Supplementary Fig. S6; see Supplementary Data for full description).

A feedback system would be less useful if its output cannot be tuned over some range by changing its input. To explore the ability to tune the output of the feedback circuit, we next induced cells at several different E2 concentrations, scanning the full range of Pg concentrations, and measured the output fluorescence at steady state. We normalized the RFP and YFP fluorescence to the maximum fluorescence value observed (Fig. 3C) to enable comparison between the circuit variants (see Supplementary Fig. S5 for non-normalized RFP and YFP outputs).

In the presence of feedback, both RFP and YFP fluorescence display a clear dependence on E2. Increasing Pg decreased the response of the RFP/E2 relationship, whereas it increased the response of the YFP/E2 relationship (Fig. 3C). This finding suggests that the feedback circuit enables the use of E2 to specify the level of output in the circuit by mitigating changes in Pg concentration. These results indicate that negative feedback implemented through competitive displacement is a powerful method for shaping the response of circuits in cells.

Discussion

In this study, we demonstrated that *de novo* designed dimerizing systems can be used to build circuits in living cells. Specifically, we used on-target and off-target interactions of these systems to implement controllable reversibility, inducing and interrupting the activity of a TF at will. Once this basic module was established, and due to its modularity, networking it in a feedback circuit was possible.

Aided by a titratable split TF system that allowed us to measure a range of DHD interaction strengths and identify several low-affinity off-target interactions, as well as a simple model to guide our understanding of the nonintuitive properties of the DHD parts, we were able to make informed design choices as we progressed to more complex circuits. This study showcases the importance of quantitatively characterizing titratable responses of designed proteins to facilitate informed design of complex circuits.

Previous work has leveraged autoinhibitory coiled coils as a method for rapid sensing of proteolytic events.[6,8] In this arrangement, weakly interacting coiled coils are covalently fused with a linker containing a protease cleavage site. Proteolytic cleavage of the linker releases the weakly interacting coiled coil and enables a higher affinity coiled coil to interact with its binding partner and either activate or deactivate a split protein. Although this system is a powerful method for coupling post-translational sensing to digital logic, the irreversible nature of proteolytic cleavage presents a major obstacle to using this motif in dynamic signaling circuits.

Others have demonstrated that competitive displacement can be used to construct dynamic signaling circuits. Bashor et al. constructed accelerator and delay circuits by inducibly expressing signaling modulators fused to high-affinity binders to outcompete a low-affinity binder, thus modifying the dynamics of the yeast mating pathway.[16] The endogenous regulators used in this study are active even in the absence of the additional heterodimerization components, making it difficult to separate the effect of inducible expression of the regulators from the effect of the variable affinity heterodimerization domains.

By contrast, the split TF system used in our study exhibits no activity in the absence of additional heterodimerization domains. Therefore, our DN negative feedback circuit is a more minimal demonstration that competitive displacement can be used to regulate dynamic behavior in a synthetic system.

One drawback of the DN motif described in our study is that using off-target interactions to reconstitute the split TF results in a weaker output than a high-affinity interaction. These interactions limit limited the dynamic range in the feedback circuit, as the dynamic range of pZ3 is small when the expression level of Z3PM is low.[28] We partially addressed this drawback by including two copies of the pZ3-YFP-cODC output in each circuit. This downside could be further addressed by using a stronger DHDoff interaction, different iSynTFs in the circuit, or by using stronger ADs, DBDs, or promoters in the split TF system.

The DN motif we describe in this study could be applied to control the activity of other split proteins beyond the split TF. Of note, multiple split Cas9 variants have been constructed that rely on chemically induced dimerization to rescue nuclease activity.[32,33] DHDs could substitute for chemical dimerization domains to activate split Cas9, and competitive displacement could enable reversible control of gene editing. Furthermore, multiple therapeutically relevant split kinases and phosphatases have been developed.[34,35] With multiple sensors and orthogonal DNs, post-translational circuits could be developed to dynamically control phosphorylation and dephosphorylation events in a cell through competitive displacement.[36]

Lastly, the modularity of the DN motif enables its use in other circuit topologies beyond negative feedback, such as incoherent feedforward loops, which require at least one inhibitory reaction.[37] Alternatively, the DN motif could be used to generate positive feedback by fusing an AD or DBD to the DN species. In this circuit, displacement of the off-target interaction would result in more powerful activation of the split TF to reinforce expression of the DN. Competitive displacement is a powerful tool for controlling split protein signaling and has many potential applications in building genetic and protein circuits that can expand the scope for biotechnology.

The Bigger Picture

Inspired by naturally evolved regulation strategies utilizing dynamic dimerization, we developed a method for controlling the activity of split proteins through competitive displacement of DHDs. Split proteins are ubiquitous, and a variety of engineered cytokines, synthetic receptors, and Cas9 variants have been published. Furthermore, DHDs have been demonstrated to function in a variety of contexts, including mammalian cells, suggesting our regulation strategy could be easily translated to biotechnology applications such as cancer immunotherapy, cellular therapy, and gene editing.

This study serves as a roadmap for the potential of protein design to enhance the capabilities of synthetic biology. We imagine a future in which the design of biomolecular circuits begins with the *de novo* rational design of its protein (or other molecular) components. Synergy between these two fields will propel future advancements in biotechnology, paving the way for safer and more effective therapies.

Materials and Methods

Media

Overnight yeast cultures were grown in YPD (1% w/v bacto-yeast extract; 2% w/v bacto-peptone; and 2% w/v dextrose). Yeast transformation cultures were diluted in YPD. Cultures for flow cytometry experiments were diluted in SDC (0.67% w/v Difco yeast nitrogen base without amino acids; 0.2% complete supplement mixture [MP Biomedicals]; and 2% w/v dextrose). SDC agar plates with the appropriate nutrient removed (Teknova) were used for selection after transformation.

Plasmid and strain construction

All plasmids were constructed using the Yeast Toolkit standard for hierarchical Golden Gate assembly.[38] The enzymes BsaI-HF v2 (NEB), T4 DNA ligase (NEB), and Esp3I FastDigest (Thermo Fisher Scientific) were used for these reactions. Sequences for the DHDs were provided by Zibo Chen and the Baker laboratory and ordered as gBlocks (IDT).[26] Sequences for the SynTF ZF43_8 were provided by the Khalil laboratory and PCR amplified using Q5 High-Fidelity 2x Master Mix (NEB).[14] All DNA manipulations were performed with standard molecular biology techniques. A list of all plasmids used can be found in Supplementary Table S1. A list of oligos used to construct parts can be found in Supplementary Table S2.

Yeast transformations were performed as previously described.[28] A list of all strains used can be found in Supplementary Table S3.

Flow cytometry experiments

Yeast strains were streaked out onto YPD plates from glycerol stocks, except for the all-by-all matrix experiment, where three transformation colonies were tested. Individual colonies were picked into 1 mL of YPD in a 2-mL V-bottomed 96-well block (Corning/Costar) for overnight growth at 30°C and 900 rpm in a Multitron shaker (Infors HT). After overnight growth, strains were diluted 1:500 in SDC and 400 μL and then were aliquoted into a new 96-well block for a 2-h outgrowth. For the all-by-all matrix, cultures were diluted 1:200 in SDC.

For the termini fusion experiment (Fig. 1B), dilutions were done in 12 mL SDC in an 8-row block and aliquoted into the rows of a 96-well block. For the 2D inductions of individual interactions (Fig. 1C), dilutions were done in 15 mL in a 50 mL trough (Corning) and aliquoted across the rows of the 96-well block. For the all-by-all matrix experiment (Fig. 1D and Supplementary Fig. S2), dilutions were done in 400 μL in a new 96-well block.

For the competition and reversibility assays (Fig. 2), dilutions were done in 12 mL in an 8-row block and aliquoted across the rows of the 96-well block.

For the feedback experiments (Fig. 3 and Supplementary Fig. S5), dilutions were done in 45 mL in a 50 mL trough and aliquoted across the rows of the 96-well block.

During the 2 h outgrowth, E2 (Sigma-Aldrich) and Pg (Fisher Scientific) induction gradients were prepared. Ten times concentrated solutions were made in fresh SDC from 36 μM (E2) and 32 μM (Pg) stock solutions. Gradients were either one-to-one (Fig. 2) or one-to-three (Figs. 1C and 3) serial diluted from a maximum induction solution. After the 2-h outgrowth, 50 μL of the corresponding solution was added to the appropriate wells at the appropriate times.

For all experiments except those shown in Figure 2F, both solutions were added at the same time, and then blocks were returned to the shaker until measurement. For Figure 2F, the E2 solutions were added after the outgrowth, and the blocks were returned to the shaker for a 4-h activation period. Then, the Pg solutions were added to induce the DN.

For the orientation experiment (Fig. 1), inductions were incubated for 6 h before measurement. For the all-by-all matrix experiment, inductions were incubated for 6 h. For experiments shown in Figure 2D–E, inductions were incubated for 6 h. For experiments shown in Figure 2F, Pg inductions were incubated for 4 h. For the dynamics shown in Figure 2F, inductions were measured every 30 min for 4 h beginning immediately after induction of the DN. For the feedback experiments, inductions were incubated for 7.5–8.5 h.

After the requisite induction times, the cultures were prepared for flow cytometry. One hundred microliters of culture was mixed with 100 μL of fresh SDC in a 96-well U-bottomed microplate (greiner bio-one). Samples were measured on a BD LSRFortessa X20 (BD Biosciences) using a high-throughput sampler. YFP/Venus fluorescence was measured using the FITC-H channel (voltage = 473). RFP/mScarlet fluorescence was measured using the PE-CF594-H channel (voltage = 709). Measurements were normalized by dividing by SSC-H (voltage = 192). For the feedback circuit experiments, compensation was performed with the FACSDiva software using an YFP benchmark strain (yAHN184) and RFP benchmark strain (yAHN642). Compensation values are listed in Supplementary Table S5.

Analysis was performed with Python 3.7 and custom scripts using the FlowCytometryTools package. All experiments were performed with biological triplicates. Reported values represent the mean and standard deviation of median normalized fluorescence values of the individual replicate populations. For the experiments where fluorescence values are normalized to an intraexperiment max (Figs. 2F and 3C), background fluorescence was subtracted out and the resultant values were divided by the indicated max of the experiment.

Growth assay

Measurement of growth was performed in parallel with the steady state measurements of the feedback circuit. Immediately after induction, 200 μL aliquots of each circuit with the indicated inducers (144 nM E2 and/or 1024 nM Pg), along with the background (WT) strain, were transferred to a Costar polystyrene tissue culture-treated 96-well assay plate with a clear flat bottom (Corning 3904) and sealed with a Breathe-Easy sealing membrane. Cultures were placed in the middle of the plate to avoid edge effects. The plate was then placed in a Spark 10M plate reader and optical density 600 nm (OD_{600}) was measured every 30 min for 24 h (Spark Control v2.2). The cultures were maintained at 30°C with double orbital shaking.

Authors' Contributions

T.H.N., G.D., H.E.-S, and A.H.N. designed the study and experiments. T.H.N. and G.D. performed plasmid and strain construction, and performed experiments. M.G.-S. and M.W. developed the computational models and performed simulations. Z.C., R.K., and D.B. designed *de novo* heterodimers and gave feedback throughout. T.H.N., G.D., M.G.-S, H.E.-S, and A.H.N. wrote and edited the article, and all authors approved the article.

Acknowledgments

The authors thank the members of the El-Samad laboratory for helpful comments on the project.

Disclaimer

The content and information does not necessarily reflect the position or the policy of the government, and no official endorsement should be inferred.

Author Disclosure Statement

T.H.N., G.D., H.E.-S, and A.H.N. are coinventors on a patent application related to this study. A.H.N. is an employee of and holds equity in Outpace Bio. H.E-.S is an investigator in the Chan Zuckerberg Biohub.

Funding Information

This research was supported by a generous gift from Mrs. Barbara Bass Bakar through the Gerson and Barbara Bakar Philanthropic Fund and the Defense Advanced Research Projects Agency [Grant No. HR0011-16-2-0045 to H.E-.S]. M.G.-S. was supported by ANID—Millennium Science Initiative Program—Millennium Institute for Integrative Biology (iBio ICN17＼_022).

Supplementary Material

Supplementary Data
Supplementary Figure S1
Supplementary Figure S2
Supplementary Figure S3
Supplementary Figure S4
Supplementary Figure S5
Supplementary Figure S6
Supplementary Table S1
Supplementary Table S2
Supplementary Table S3
Supplementary Table S4
Supplementary Table S5

References

1. Klemm JD, Schreiber SL, Crabtree GR. Dimerization as a regulatory mechanism in signal transduction. *Annu Rev Immunol*. 1998;16:569–592. DOI: 10.1146/annurev.immunol.16.1.569.
2. Jones S. An overview of the basic helix-loop-helix proteins. *Genome Biol*. 2004;5:1–6. DOI: 10.1186/gb-2004-5-6-226.
3. Benezra R, Davis RL, Lockshon D, et al. The protein Id: a negative regulator of helix-loop-helix DNA binding proteins. *Cell*. 1990;61:49–59. DOI: 10.1016/0092-8674(90)90214-y.
4. Sun XH, Copeland NG, Jenkins NA, et al. Id proteins Id1 and Id2 selectively inhibit DNA binding by one class of helix-loop-helix proteins. *Mol Cell Biol*. 1991;11:5603–5611. DOI: 10.1128/mcb.11.11.5603.
5. Lebar T, Lainšček D, Merljak E, et al. A tunable orthogonal coiled-coil interaction toolbox for engineering mammalian cells. *Nat Chem Biol*. 2020;16:513–519. DOI: 10.1038/s41589-019-0443-y.
6. Shekhawat SS, Porter JR, Sriprasad A, et al. An autoinhibited coiled-coil design strategy for split-protein protease sensors. *J Am Chem Soc*. 2009;131:15284–15290. DOI: 10.1021/ja9050857.
7. Gao XJ, Chong LS, Kim MS, et al. Programmable protein circuits in living cells. *Science*. 2018;361:1252–1258. DOI: 10.1126/science.aat5062.
8. Fink T, Lonzarić J, Praznik A, et al. Design of fast proteolysis-based signaling and logic circuits in mammalian cells. *Nat Chem Biol*. 2019;15:115–122. DOI: 10.1038/s41589-018-0181-6.
9. Lee MJ, Mantell J, Hodgson L, et al. Engineered synthetic scaffolds for organizing proteins within the bacterial cytoplasm. *Nat Chem Biol*. 2017;14:142–147. DOI: 10.1038/nchembio.2535.
10. Lee MJ, Mantell J, Brown IR, et al. De novo targeting to the cytoplasmic and luminal side of bacterial microcompartments. *Nat Commun*. 2018;9:1–11. DOI: 10.1038/s41467-018-05922-x.
11. Dueber JE, Yeh BJ, Chak K, et al. Reprogramming control of an allosteric signaling switch through modular recombination. *Science*. 2003;301:1904–1908. DOI: 10.1126/science.1085945.
12. Dueber JE, Mirsky EA, Lim WA. Engineering synthetic signaling proteins with ultrasensitive input/output control. *Nat Biotechnol*. 2007;25:660–662. DOI: 10.1038/nbt1308.
13. Buchler NE, Cross FR. Protein sequestration generates a flexible ultrasensitive response in a genetic network. *Mol Syst Biol*. 2009;5:272. DOI: 10.1038/msb.2009.30.
14. Khalil AS, Lu TK, Bashor CJ, et al. A synthetic biology framework for programming eukaryotic transcription functions. *Cell*. 2012;150:647–658. DOI: 10.1016/j.cell.2012.05.045.
15. Bashor CJ, Patel N, Choubey S, et al. Complex signal processing in synthetic gene circuits using cooperative regulatory assemblies. *Science*. 2019;364:593–597. DOI: 10.1126/science.aau8287.
16. Bashor CJ, Helman NC, Yan S, et al. Using engineered scaffold interactions to reshape MAP kinase pathway signaling dynamics. *Science*. 2008;319:1539–1543. DOI: 10.1126/science.1151153.
17. Whitaker WR, Davis SA, Arkin AP, et al. Engineering robust control of two-component system phosphotransfer using modular scaffolds. *Proc Natl Acad Sci U S A*. 2012;109:18090–18095. DOI: 10.1073/pnas.1209230109.
18. Ryu J, Park S-H. Simple synthetic protein scaffolds can create adjustable artificial MAPK circuits in yeast and mammalian cells. *Sci Signal*. 2015;8:ra66. DOI: 10.1126/scisignal.aab3397.
19. Groves B, Khakhar A, Nadel CM, et al. Rewiring MAP kinases in Saccharomyces cerevisiae to regulate novel targets through ubiquitination. *Elife*. 5 [Epub ahead of print]; DOI: 10.7554/eLife.15200.
20. Dueber JE, Wu GC, Malmirchegini GR, et al. Synthetic protein scaffolds provide modular control over metabolic flux. *Nat Biotechnol*. 2009;27:753–759. DOI: 10.1038/nbt.1557.
21. Thomik T, Wittig I, Choe J-Y, et al. An artificial transport metabolon facilitates improved substrate utilization in yeast. *Nat Chem Biol*. 2017;13:1158–1163. DOI: 10.1038/nchembio.2457.
22. Klaus M, D'Souza AD, Nivina A, et al. Engineering of chimeric polyketide synthases using SYNZIP docking domains. *ACS Chem Biol*. 2019;14:426–433. DOI: 10.1021/acschembio.8b01060
23. Cho JH, Collins JJ, Wong WW. Universal chimeric antigen receptors for multiplexed and logical control of T cell responses. *Cell*. 2018;173:1426–1438.e11. DOI: 10.1016/j.cell.2018.03.038.
24. Chen Z, Kibler RD, Hunt A, et al. De novo design of protein logic gates. *Science*. 2020;368:78–84. DOI: 10.1126/science.aay2790.
25. Thompson KE, Bashor CJ, Lim WA, et al. SYNZIP protein interaction toolbox: in vitro and in vivo specifications of heterospecific coiled-coil interaction domains. *ACS Synth Biol*. 2012;1:118–129. DOI: 10.1021/sb200015u.
26. Chen Z, Boyken SE, Jia M, et al. Programmable design of orthogonal protein heterodimers. *Nature*. 2019;565:106–111. DOI: 10.1038/s41586-018-0802-y.
27. Aranda-Díaz A, Mace K, Zuleta I, et al. Robust synthetic circuits for two-dimensional control of gene expression in yeast. *ACS Synth Biol*. 2017;6:545–554. DOI: 10.1021/acssynbio.6b00251.
28. Gómez-Schiavon M, Dods G, El-Samad H, et al. Multidimensional characterization of parts enhances modeling accuracy in genetic circuits. *ACS Synth Biol*. 2020;9:2917–2926. DOI: 10.1021/acssynbio.0c00288.
29. Saiz-Baggetto S, Méndez E, Quilis I, et al. Chimeric proteins tagged with specific 3xHA cassettes may present instability and functional problems. *PLoS One*. 2017;12:e0183067. DOI: 10.1371/journal.pone.0183067.
30. Lee S, Lim WA, Thorn KS. Improved blue, green, and red fluorescent protein tagging vectors for *S. cerevisiae*. *PLoS One*. 2013;8:e67902. DOI: 10.1371/journal.pone.0067902.

31. Ng AH, Nguyen TH, Gómez-Schiavon M, et al. Modular and tunable biological feedback control using a de novo protein switch. *Nature*. 2019;572:265–269. DOI: 10.1038/s41586-019-1425-7.
32. Wright AV, Sternberg SH, Taylor DW, et al. Rational design of a split-Cas9 enzyme complex. *Proc Natl Acad Sci U S A*. 2015;112:2984–2989. DOI: 10.1073/pnas.1501698112.
33. Nguyen DP, Miyaoka Y, Gilbert LA, et al. Ligand-binding domains of nuclear receptors facilitate tight control of split CRISPR activity. *Nat Commun*. 2016;7:12009. DOI: 10.1038/ncomms12009.
34. Camacho-Soto K, Castillo-Montoya J, Tye B, et al. Small molecule gated split-tyrosine phosphatases and orthogonal split-tyrosine kinases. *J Am Chem Soc*. 2014;136:17078–17086. DOI: 10.1021/ja5080745
35. Diaz JE, Morgan CW, Minogue CE, et al. A split-Abl kinase for direct activation in cells. *Cell Chem Biol*. 2017;24:1250–1258.e4. DOI: 10.1016/j.chembiol.2017.08.007.
36. Mishra D, Bepler T, Teague B, et al. An engineered protein-phosphorylation toggle network with implications for endogenous network discovery. Science 373 [Epub ahead of print]; DOI: 10.1126/science.aav0780.
37. Alon U. Network motifs: theory and experimental approaches. *Nat Rev Genet*. 2007;8:450–461. DOI: 10.1038/nrg2102.
38. Lee ME, DeLoache WC, Cervantes B, et al. A highly characterized yeast toolkit for modular, multipart assembly. *ACS Synth Biol*. 2015;4:975–986. DOI: 10.1021/sb500366v.